A Wearable Flexible Energy-Autonomous Filtenna for Ethanol Detection at 2.45 GHz

(Article begins on next page)

07 November 2024

A Wearable Flexible Energy-Autonomous Filtenna for Ethanol Detection at 2.45 GHz

Francesca Benassi, *Graduate Student Member, IEEE,* Giacomo Paolini, *Graduate Student Member, IEEE,* Diego Masotti, *Senior Member, IEEE,* and Alessandra Costanzo, *Senior Member, IEEE*

Abstract—This work proposes the design and implementation of a wearable rectifying filtenna (filtering antenna) which is activated and powered wirelessly, to detect the presence of ethanol solutions. The system is implemented on a Rogers RT/Duroid 5880 substrate (ε_r = 2.2, thickness: 0.508 mm), whose flexibility facilitates the system wearability. The fluid detection is performed by a resonant stub embedding a microfluidic channel on its end, which resonates as an open circuit at 2.45 GHz, when the channel is filled with the ethanol solution, and undergoes a dramatic shift on its input impedance behavior when the channel is filled with water or when it is empty. The system is powered wirelessly by means of a 2.45 GHz narrowband antenna and the frequency selection is performed by a second order open end coupled-line filter whose one end is loaded with the resonant stub. The filtenna RF-signal is transduced by a full-wave rectifier exploiting low-threshold voltage diodes and fluid detection is read out through different values of dc-output voltages, allowing an immediate response. The system is designed and optimized by means of full-wave/nonlinear co-simulations and the realized prototype is measured to confirm a safe detection of the tested solution.

Index Terms—Filtenna, Microfluidic, Wearable Sensor, WPT.

I. Introduction

IN the last few years, microwave dielectric spectroscopy has become a possible alternative to physical or chemical transduction methods, when labeling protocols or biological markers are not necessary [1], avoiding the use of large amount of samples, reagents, solvents and also time. Among the non-invasive and non-destructive techniques, such approach is considered a valid procedure for investigating biological liquids, molecules and cells, especially when a quick characterization of a biological or chemical fluid is required. Indeed, in the GHz-band, the electromagnetic waves can penetrate into cellular membranes and establish interaction with biological matters. This allows not only to correlate the variation of dielectric permittivity and permeability to different types of cells, but also to develop new techniques to enable early diagnosis of severe diseases [2]. This label-free and contactless approach exploits the dielectric characterization using

F. Benassi, G. Paolini and D. Masotti are with the Department of Electrical, Electronic and Information Engineering Guglielmo Marconi (DEI), University of Bologna, 40136 Bologna, Italy (e-mail: francesca.benassi9@unibo.it; giacomo.paolini4@unibo.it; diego.masotti@unibo.it).

A. Costanzo is with the Department of Electrical, Electronic and Information Engineering Guglielmo Marconi (DEI), University of Bologna, 47522 Cesena, Italy (e-mail: alessandra.costanzo@unibo.it).
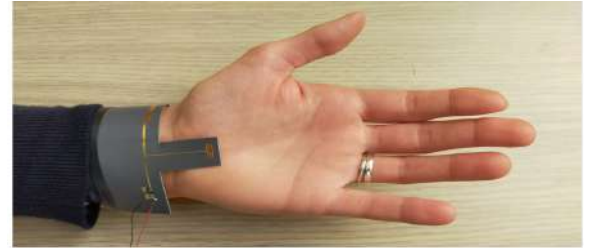
Fig. 1. Photo of the wearable wireless ethanol detector: (a) the receiving antenna is connected to (b) a coupled-line filterloaded with the microfluidic channel and rectifier circuity.

microwave technology within a new scenario, which is less industrial and more medical. The operating principle on which these new methods are based is the analysis of dielectric properties of tested solutions when exposed to an electromagnetic field at different frequencies. The same concept can also be applied in the opposite way: the presence of a specific fluid modifies the dielectric properties of a material causing a shift on its resonance frequency. This behavior has been successfully exploited to create a chipless humidity sensor for wearable devices scenario [3].

These properties have already been exploited in several laboratory implementations using modified microwave components, such as interdigitated capacitor as sensing resonator [4], where the capacitance value is strictly dependent on the ε_r of the matter interposed between the conductors. Moreover, planar technology has been exploited as microwave sensor to realize miniaturized structures [5]–[7], suitable for testing small volumes of liquids in the micro or nano-liter scale in a laboratory environments. Furthermore, not only medical and scientific environments find in microfluidic sensors various useful applications, but also industrial protocols for liquid quality control [8], which are carried out exploiting advanced reflectometry principles. Combining liquids and electromagnetic waves has been demonstrated to be a consolidated proce-

dure to perform cell-scale analysis [9] in a range from 10 GHz to 20 GHz, or even higher as in [10], where the exploitation of a millimeter-wave coplanar transmission line equipped with a microfluidic channel, placed on top of it, allows to identify specific types of cells, in particular human umbilical vein endothelial cells. In [11] a miniaturized sensor, working in the range from 40 MHz to 40 GHz, is presented. The main advantage resides in the in-culture medium analysis of cell and in the single-cell detection and identification. The sensing area has been derived on an interdigitated capacitor, as in [12]–[15], where the interactions between the electromagnetic field and the fluid under test take place. Other reference structures that have been adopted consist of a T-resonator [16] with a small rectangular microfluidic channel in which the fluid is directly provided with small pipes. Recent implementations exploit 3D-printing manufacturing technology to create such microwave microfluidic sensors able to derive the electrical properties of specific fluids [17], as in [18] where it has been exploited to detect water-ethanol concentration by means of a high-Q resonator filled with different solution concentrations by means of small pipes. This methodology allows to discriminate small variation in the solutions concentration up to 0.1% of ethanol.

Recently, coupled-line sensors have been used for effective permittivity measurements, enabling the sensing of dielectric properties for both liquids and solids [19]–[21].
Most of these studies have been carried out in a laboratory environment, with controlled powering of the sensors as well as fluids filling. In this work, which is based on a preliminary design presented in [22], it is demonstrated a new fully energy-autonomous microwave system, which does not need to operate in controlled laboratory conditions and can be worn as a bracelet to wirelessly detect the presence of ethanol solutions. It is therefore configured as a flexible system for the rapid control of personal hygiene that is to identify the presence or absence of the searched solution, rather then to quantify the ethanol concentration inside the solution. Practical applications can be found in hospital environments in which the hand sanitation is the simplest but one of the most effective way to prevent undesired infections, and to reduce the spread of antibiotic-resistant microorganisms. In this scenario, such system could be used to check the correct hand sanitation procedure of the hospital personnel, right after the application of a hand sanitizer. For this reason the realized system aims to be a cheap easy-to-be worn device for screening purposes, rather than a sensor able to precisely detect ethanol concentration inside an antiseptic solution. To describe a simple case scenario: a person inside the hospital has performed hands sanitization using an alcohol-based hand sanitizer gel while wearing the proposed system as shown in the photos of Fig. 1. Subsequently, the sanitization is checked by placing his/her hand under a gate equipped with a reader that provides the RF power to activate the detection. In order to cover a broad range of commercial antiseptic sanitizers, a solution with an ethanol concentration of 70% has been chosen: the stub is designed to resonate when the channel is filled with such solution, thus providing sharp variation of its input impedance with different fluids fillings. The correlation

between fluid dielectric properties and the frequency shift for resonant structures is a well-known point, this is why the originality of this proposed work relies on the exploitation of this principles to create a system whose readout is not strictly related to the use of laboratory instruments, but can be fully passive. One innovative aspect of the proposed system is to load one open-end of a band-pass coupled line filter, centered around 2.45 GHz, with the stub embedding the microfluidic channel, thus reaching the twofold goal of linking the filter frequency behavior to the channel filling and of enhancing such frequency selectivity with respect to previous planar realizations [19].

The latter characteristic enables another innovative feature of the sensor, that is energy autonomy. Indeed, the loaded-filter is connected on one end to a narrowband antenna, realizing a filtenna, and on the other to a rectifier, which seamlessly provides the fluid detection in terms of output dc rectified voltage levels. As will be clarified in the following, it is the whole system architecture, including the filtenna choice, that allows a fully passive wearable detection.

A representation of the proposed system is displayed in Fig. 1: a flexible substrate allows the system to be worn and to perform the detection when placed on the body surface. With respect to the first idea presented in [22], the present system enhances the sensor response to different fluids, by a meandered design of the microfluidic channel, and provides the nonlinear design of the filtenna for simultaneous frequency selection and matching with the rectifier, avoiding the need for an additional matching networks. A thicker substrate than in [22] (0.508 mm) has been chosen to enhance the antenna performance in terms of gain, without loosing the flexibility characteristics. The energy-autonomous wireless detector has been prototyped and experimentally characterized by means of an extensive measurements campaign: the sensor read-out is demonstrated by measuring its response to the presence of different fluids, that are clearly transduced by the variation of the dc-output voltages on the load.

II. Design of a Microwave Resonator Embedding the Microfluidic Channel

A microstrip technology has been selected for realizing the whole system on a unique quite flexible substrate. A Rogers RT/Duroid 5880, with a thickness of 0.508 mm, has been chosen as the best compromise among compactness, antenna radiation efficiency and microfluidic channel volume. The microfluidic channel, has been dug into the substrate and it is used as the medium between two planar metals that make up artificial end capacitance of a microstrip open stub. In order to extend the sensing area, a meandered configuration has been chosen as shown in Fig. 2. The introduction of a meandered channel, compared to a simple rectangular one, allows to maintain a relatively compact structure and to simultaneously extend the sensing area. This implementation allows to increase the effectiveness of the modified stub because of larger resonant frequency shifts, with respect to the filling media, and higher resonator Q-factor. When the fluid fills the channel, the interdigitated capacitor experiences a variation on
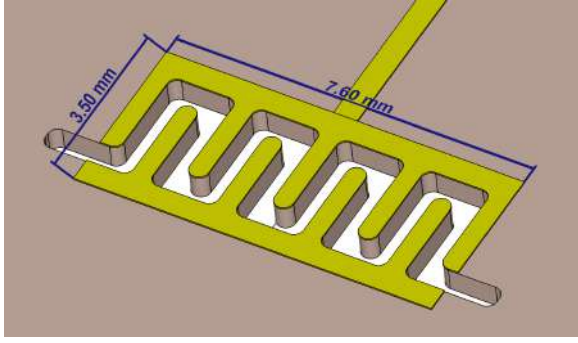
Fig. 2. Representation of the microfluidic channel realized as an interdigitated capacitor to enhance the sensitivity during fluid detection.
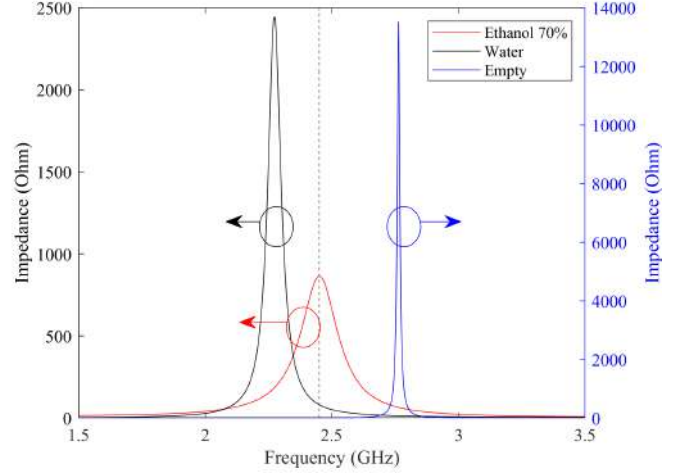

Fig. 3. Frequency behavior of the real part of the modified open end stub input impedance with the channel filled with different fluids.
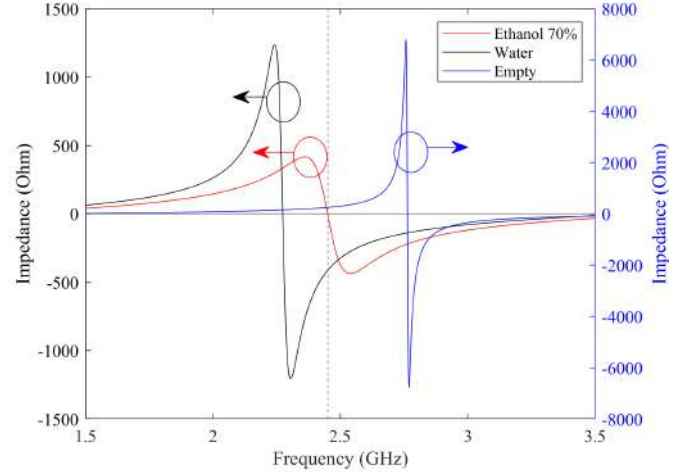

Fig. 4. Frequency behavior of the imaginary part of the modified open end stub input impedance with the channel filled with different fluids.

its capacitance due to the different ϵ_r of the material interposed between the fingers.

The well-known correlation between the stub length and its resonant frequency allows to easily tune a stub as an open circuit at a specific resonant frequency. In the presented implementation, the stub ends with the interdigitated capacitor embedding the microfluidic channel, therefore the electrical length of the stub is determined by the fluids filling the channel which have different dielectric properties. This variation on the electrical length causes a shift on the resonant frequency of the stub that can be exploited to perform the sensing. To detect ethanol solution properly, the stub is tuned to open resonate at 2.45 GHz when the channel is filled with a reference water-ethanol solution, in particular a solution made of 70% ethanol and 30% water. For the present implementation, the resulting stub length is 32.8 mm and the channel volume is 7.4 mm^3. After tuning the stub to open-resonate at the frequency of 2.45 GHz in the presence of the water-ethanol solution, the fluid is firstly substituted with water to identify the absence of ethanol in a solution and then with air, to simulate the empty channel. The different dielectric characteristics of the inter-changed fluids cause a shift in the stub resonant frequency; thus for the operating frequency of 2.45 GHz, in the presence of water or empty channel, the stub does not perform as an open circuit. This variation can be observed when comparing the real and imaginary parts of the stub input impedance for the three fluids, as shown in Fig. 3 and Fig. 4. Due to the dielectric properties of each fluid, reported in Table I, and in particular to the related losses, the real part of the input impedance varies not only in terms of resonant frequency but also in terms of absolute value, as it can be clearly seen for the empty channel case. However, since the shift in frequency for the three fluids is very large, this difference in terms of absolute value does not affect the sensing operation of the system. It is also important to notice that, since the system has been designed to perform the sensing when placed on the body surface, sweat can also be present. However, having implemented a capacitive resonator, thus sensitive to the fluid dielectric permittivity, implies that the difference between water and sweat does not affect the sensor performance in terms of detection sensitivity. For this reason, water at 20 degree Celsius is used for the simulations and, subsequently, for the measurement campaigns. Being this detector sensitive to the different dielectric properties of the

TABLE I
FLUIDS DIELECTRIC PROPERTIES AT 2.45 GHz [24]

Fluid	ε_r	σ
Water-ethanol 70%	30	2.18
Water	77.2	1.28
Air	1	0

tested fluid, it is worth mentioning that other solutions with the same dielectric properties could be exchanged for the searched ethanol one. However, the detector is intended to be used in a specific scenario, right after the hand sanitation with the use of common hand antiseptic solutions which contain ethanol as the main component. This confirms the main goal of this system which is the detection of the presence or absence of an ethanol solution rather that the quantification of the related concentration.

In order to assess the effective reliability of the proposed

system, one critical aspect must be underlined: the filling percentage of the channel cannot be controlled by pipes as in other related works [16], [17]. Since the system is required to be easily placed on the body surface, the sensor is entirely derived on a flexible substrate, therefore the channel filling is not controlled by pipes, but it depends on the liquid in its close proximity. In particular, since the resonance of the open stub is strictly dependent on the type of fluid contained in the microfluidic channel, but also on the filling percentage. Due to the small dimensions, the channel is expected to be completely filled by the analyzed solution; however, in case of having different filling percentage, the value of the input impedance may vary, thus investigating the effects is a necessary and preliminary step. This analysis has been performed for the sake of completeness, in order to describe the behavior of the system in a thorough way. However, the aim of this work is not to design a sensor to quantify the exact concentration of ethanol inside the tested solution, but to design a detector for screening purposes, that has the main goal of identifying the presence or the absence of common hand sanitizer solutions. Simulations are conducted for increasing percentages of the channel filling, from 25% to 100%, which correspond to a shift from an almost empty channel towards a complete full one, as described in Fig. 5 where ethanol solution is analyzed as an example.
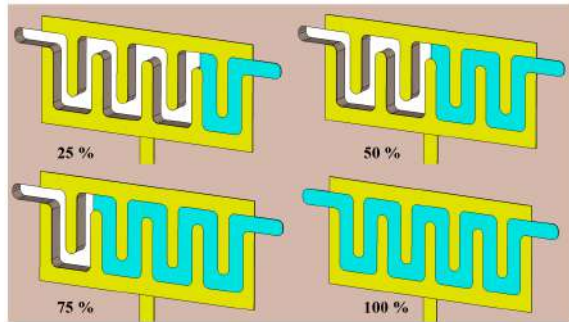

Fig. 5. Description of the different filling percentages.

As it can be expected, for a 25% filling of ethanol solution inside the channel, the resulting real part of the stub input impedance is far from the desired one at 2.45 GHz, and it is closer to the one experienced for an empty channel.

There are also intermediate combinations of filling percentage and ethanol concentration that can be investigated to analyze their effect on the output results. The analyzed cases are the following: channel half-filled with the ethanol solution for different ethanol concentrations. The ethanol concentration inside the solution is made vary from 30% to 70%, thus including one of the previous scenarios described in Fig. 5. The resulting stub input impedance, displayed in Fig. 8 and Fig. 9, shows values that are not too far from the reference one at 2.45 GHz, and they do not affect the overall system behavior as it is shown in Section IV. This means that the detector could work properly even in the presence of a partially-filled channel. However, the small dimensions of the channel would prevent this situation to happen with a high probability, but, for
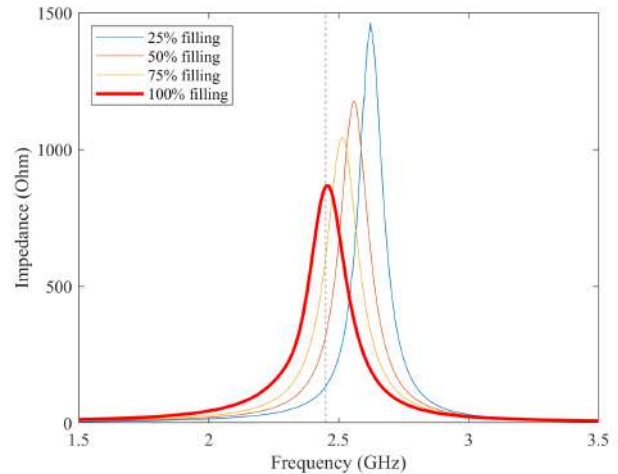

Fig. 6. Frequency behavior of the real part of the stub input impedance for different filling percentages.
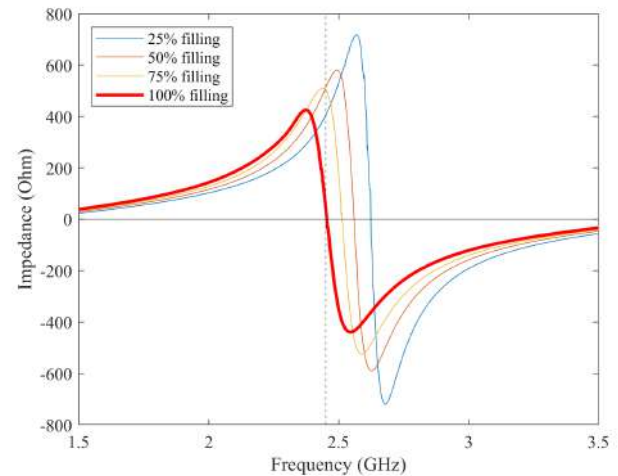

Fig. 7. Frequency behavior of the imaginary part of the stub input impedance for different filling percentages.

the sake of completeness, investigations have been conducted and reported.

For this reason, simulations and optimizations are conducted considering a microfluidic channel completely filled with the analyzed fluids. The channel filling is expected to be performed in the described way: from the bottom layer of the structure to the copper level of the interdigitated capacitor. In this way, the electrical length of the stub is modified accordingly, experiencing repeatability in the output results.

To ensure a high frequency selective behavior of the proposed sensing system, the modified open stub, embedding the microfluidic channel, is used to load a second-order coupled-line band-pass filter, substituting one of its open end terminations. In this way, the filter performance are strictly related to the channel content.
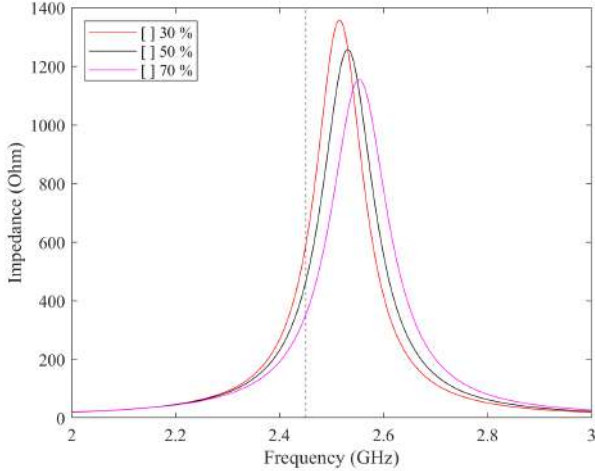
Fig. 8. Frequency behavior of the real part of the stub input impedance for a 50% filling and various ethanol concentrations inside the solution.
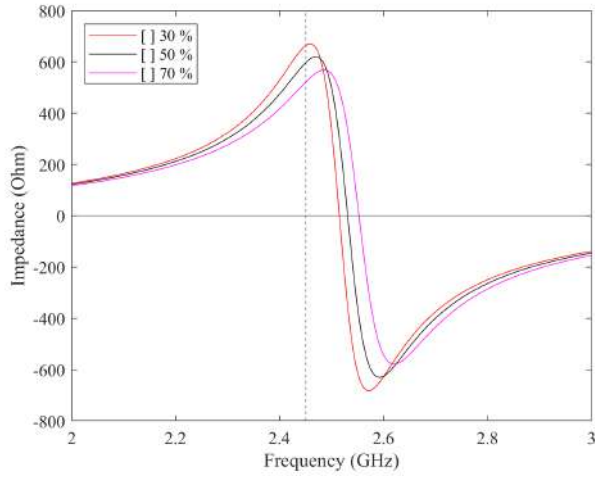

Fig. 9. Frequency behavior of the imaginary part of the stub input impedance for a 50% filling and various ethanol concentrations inside the solution.

III. WIRELESS ACTIVATION OF THE SENSOR SYSTEM READOUT

In order to create an energy autonomous identification of the channel content, the modified open stub can be inserted inside the linear subnetwork of a rectenna system to excite a full-wave rectifier whose dc voltage and power output levels become strictly related to the microfluidic channel contents. In the following, two solutions are analyzed: a T-resonator topology and a loaded band-bass filter, both embedding the modified open stub.

A. T-resonator

The rectenna topology, including the T-resonator based on the modified open stub, is shown in Fig. 10: only when the modified stub open-resonates (at the designed frequency this corresponds to the channel filled with the ethanol solution) the antenna received power is completely transferred to the rectifier input and distinguishable rectenna performance are

expected. This behavior is used to detect the the presence of ethanol solution in the channel as discussed in the previous section.
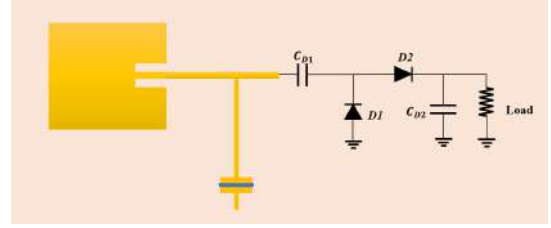

Fig. 10. Preliminary connection between the antenna and the stub.

This implementation has the advantage of having a very simple resonant network connecting the antenna to the rectifier, thus minimizing the RF power losses. Despite this, a too weak frequency-selective behavior of the resulting one-port assembly has been observed, which did not allow to transduce the channel content based on the rectifier output voltage or power. This is clearly shown in Fig. 11 where the predicted rectenna dc-output voltages are plotted with respect to the received RF power, when the channel is filled with the solutions summarized in Table I: the three curves are almost overlapped.
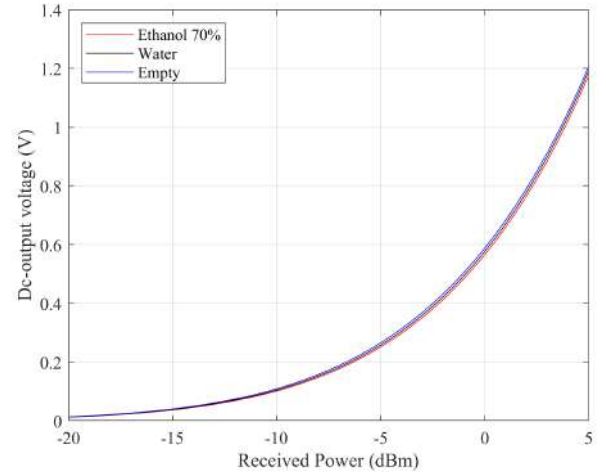

Fig. 11. Dc-output voltage for the T-resonator configuration.

B. Loaded Coupled-line Filter

To overcome the up-mentioned issue related to the lack of fluid selectivity, the system has been electrically decoupled from the patch antenna used for providing the activation power. Moreover, to also ensure a frequency-selective behavior, implementing a coupled-line filter has been the operative choice. The modified open stub, embedding the microfluidic channel, is used to load a second-order coupled-line band-pass filter, substituting one of its open end terminations. In this way, the filter performance are strictly related to the channel content. A second-order filter has been chosen since it is a good trade-off between frequency selectivity and filter

related losses: increasing the number of sections would lead to a sharper band-pass filter but with lower values of the transmission coefficients for any analyzed fluids. The sensor activation can be obtained by connecting a patch antenna to the filter input port, creating a filtenna (filtering antenna) whose frequency behavior is determined by the microfluidic channel filling. The filter output RF signal is then used to excite a full-wave rectifier whose dc voltage and power output levels become strictly related to the microfluidic channel contents. The second-order open-end coupled-line filter is derived on the same RT/Duroid 5880 substrate and the section length is in agreement with the expected value that is approximately $\lambda/4$, corresponding to about 20 mm [25]. The characteristic impedance (Z_c) of each section is 50 Ω, hence the line width is the same as the antenna feeding line one. As a preliminary analysis, a reference band-pass filter is designed for a center frequency of 2.45 GHz with ideal open ends, and its performance in terms of reflection and transmission coefficients are plotted in Fig. 12, Fig. 13 and Fig. 14.

Fig. 13. Predicted output port reflection coefficients of the reference filter and the loaded ones, with the channel filled with the different fluids.
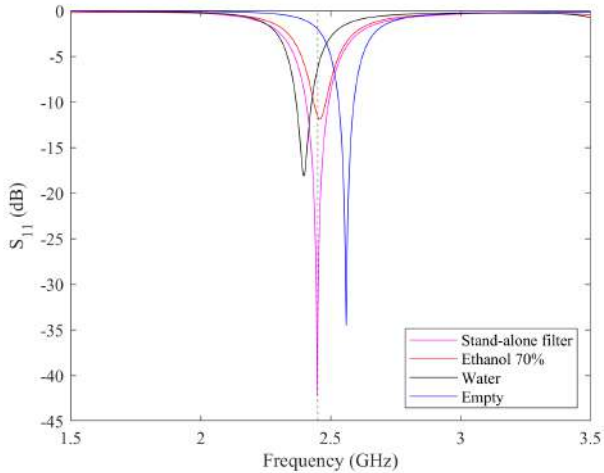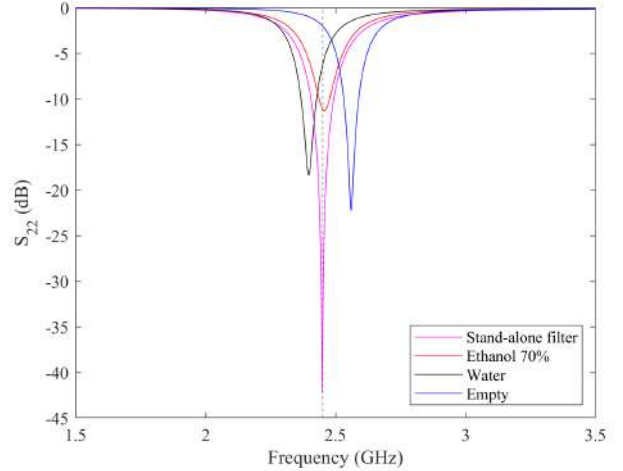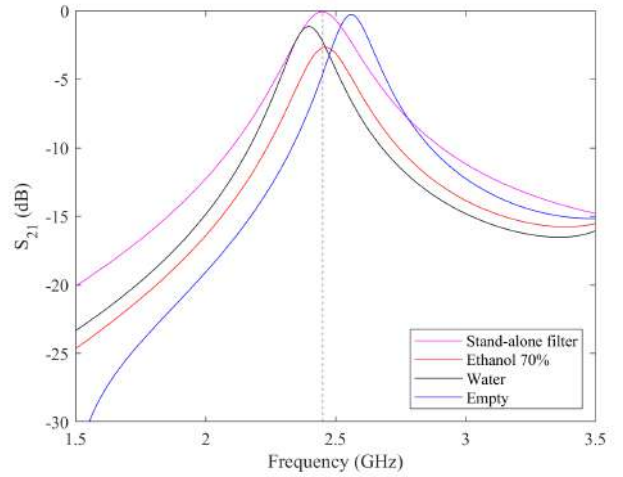

Fig. 12. Predicted input port reflection coefficients of the reference filter and the loaded ones, with the channel filled with the different fluids.

Fig. 14. Predicted transmission coefficients of the reference filter and the loaded ones, with the channel filled with the different fluids.

Subsequently, the upper line of the second section of the filter is loaded with the modified stub and three simulations are carried out with its channel filled with the reference fluids: the corresponding results are superimposed in the same figures. As expected, the closest performance to the ideal ones are achieved when the channel is filled with the ethanol solution: the transmission coefficient value is lower due to the extra losses introduced by the fluid.

C. Design of the Rectifier

First, a stand-alone rectifier is designed by means of Harmonic Balance simulations: the full-wave topology of Fig. 10 has been chosen which makes use of the Schottky diodes (Skyworks SMS-7630LF) chosen for their low threshold voltage (0.340 V) and break-down voltage of 2 V. The rectifier is optimized with the goal of maximizing the RF-to-dc efficiency over a power range, spanning from -20 dBm to 5 dBm. The optimum load is 6500 Ω and the two capacitors are equal to

47 pF. To get a good estimate of the rectifier input impedance variations, over the frequency band and the RF power range of interest, a sequence of HB simulations has been carried out and the complex ratio between the input voltage and current phasors at each fundamental frequency has been used to estimate such impedance. This nonlinear behavior is plotted in Fig. 15 with respect to the incoming RF power, for a fundamental tone of 2.45 GHz; while in Fig. 16 the same quantities for different fundamental tones are shown when the input RF power is -10 dBm.

IV. NONLINEAR OPTIMIZATION OF THE FILTENNA INTEGRATED WITH THE RECTIFIER

Since the loaded filter connects the antenna and the rectifier, a further nonlinear design step has to be carried out to provide the final topology that considers the filter optimized inside the nonlinear circuit including the antenna and the rectifier. This allows to combine filtering and matching capabilities inside the
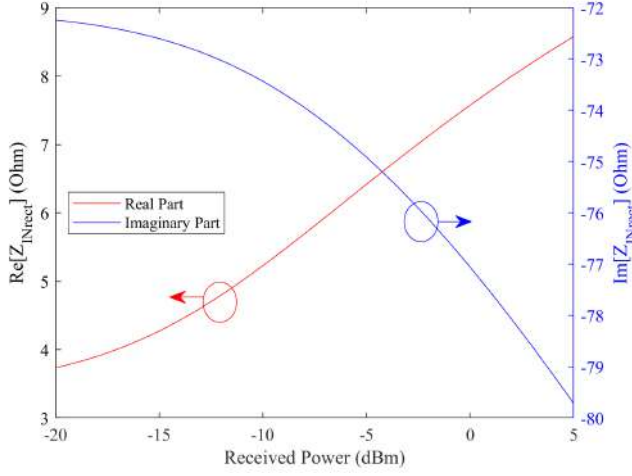
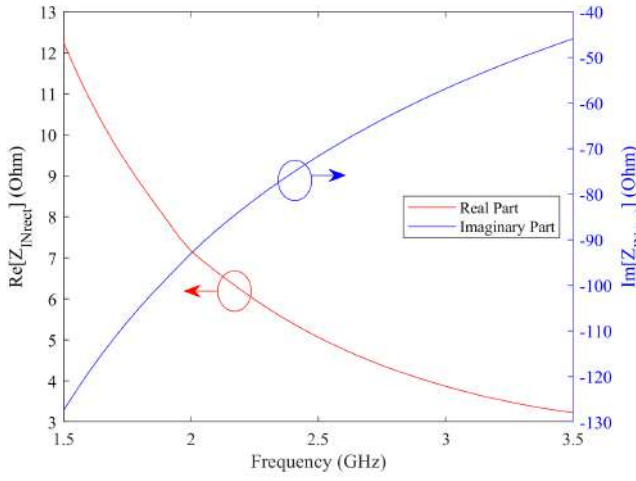Fig. 15. Predicted rectifier input impedance @ 2.45 GHz versus RF power.

Fig. 16. Predicted rectifier input impedance versus frequency, for an RF power of -10 dBm.

same component, avoiding an additional matching network. The antenna and its radiation properties must be accounted for inside the nonlinear simulation of the whole system, to accurately estimate the received power at the filter input port [26]. This is done by using the antenna radiation resistance, extracted from EM simulation, as the internal resistance of the Thevenin equivalent model of the antenna in receiving mode.

The circuit schematic of the whole system is reported in Fig. 17(a), where the reference impedances are also highlighted: Z_A is the antenna equivalent impedance and can be written as:

$$Z_A = R_A + jX_A = (R_T + R_J) + jX_A \qquad (1)$$

In R_A two contributions need be distinguished: the radiation resistance R_T and the resistance associated to ohmic losses R_J.

Z_{NL} is the nonlinear equivalent impedance of the loaded-filter and rectifier assembly; in Figs. 17(b) the corresponding equivalent circuit is shown: V_g is the voltage generator that
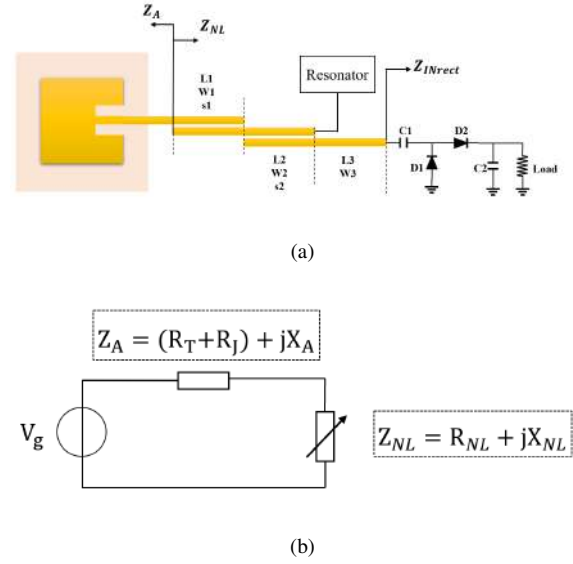

(a)

(b)

Fig. 17. (a) Circuit schematic of the designed filtenna loaded by the rectifier and (b) its equivalent representation, consisting of a Thevenin equivalent of the receiving antenna loaded by a nonlinear complex impedance.

represents the incident power on the antenna, whose internal impedance is R_A. The aim is to find the best matching conditions between the two impedances, Z_A and Z_{NL} over a large received power range, to maximize the power entering the rectifier. Indeed an ideal conjugate matching $Z_{NL} = Z_A^*$ between the antenna and the load can be obtained only for a specific frequency and received power, due to the nonlinear behavior of the rectifier given its behavior previously discussed and reported in Fig. 15 and Fig. 16.

It is noteworthy that R_T and R_J need be distinguished, in order to correctly predict the actual received power by the antenna. This can be obtained using the antenna radiation efficiency, available from the EM simulation, that can be expressed as:

$$\delta = \frac{P_{RF}}{P_I} \qquad (2)$$

where P_{RF} is the power delivered to the load, that for the present case corresponds to the available power at the coupled-line filter input, and P_I is the power incident on the antenna. By using R_T and R_J, δ can be equivalently represented as:

$$\delta = \frac{R_T}{R_A} = \frac{R_T}{R_T + R_J} \qquad (3)$$

From (3), it is possible to derive the radiation resistance R_T to be used in the antenna circuit model for computing the effective received power. For the present case, the EM analysis of the filtenna resulted in $\delta = 64\%$ from which a radiation resistance $R_T = 32\ \Omega$ is derived (with $R_A = 50\ \Omega$).

This procedure enables the realistic prediction of the antenna received power and of the actual power at the rectifier input, which can significantly differ especially for low-efficiency antennas. Otherwise an overestimation of the received power occurs, causing a shift of the overall performance towards lower received power, as shown in Fig. 18 where the rectenna

dc voltage is computed using R_T and R_A as the internal impedances of the voltage generator of Fig. 17(b), respectively.
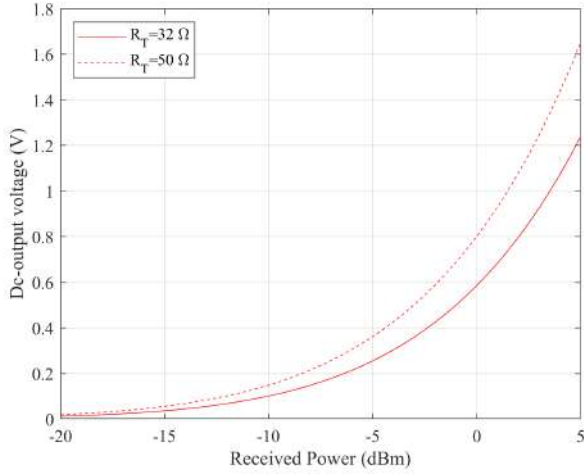

Fig. 18. Comparison between the predicted rectenna dc-output voltages for the same filtenna conditions (the channel is filled with the same fluid) when the antenna efficiency is accounted for (solid line) and when it is neglected (dashed line).

The patch antenna has been first designed and characterized separately: its narrow-band characteristic allows to select the correct operating frequency for fluid sensing purposes. The antenna is derived on the same flexible substrate, Rogers RT/duroid 5880, and it is characterized by a 5.54 dBi gain.

The EM characterization of the patch antenna is described in terms of S-parameter derived from EM simulations, and the predicted received power is modeled through a RF voltage source as discussed above.

The optimization is conducted by means of Harmonic Balance/nonlinear simulations [27], [28] with the goals of maximizing the $\eta_{RF-to-dc}$ and dc-output voltage in the presence of the ethanol solution in the loaded filter. All the filter geometrical parameters are used as optimization variables, starting from a symmetrical topology.
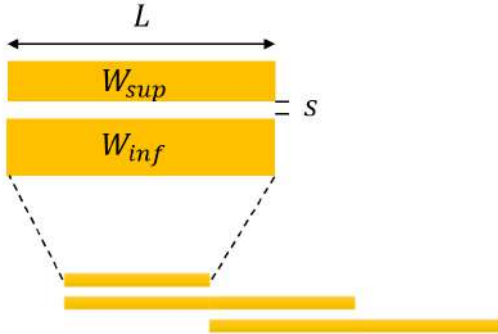

Fig. 19. Representation of an asymmetrical coupled line used in the presented implementation.

Subsequently, the use of asymmetrical coupled lines, as in Fig. 19, has provided useful degrees of freedom to achieve a better matching between the antenna and the rectifier [29]. The

circuital optimization has been carried out with real models of the lumped element components.

Fig. 20 shows the simulated dc-output voltages, versus the received RF power, when the channel is filled with the three fluids of interest: the results clearly show that the system is able to identify these fluids by providing at the rectifier output three different dc voltages, for a broad range of received power. The corresponding dc-output power on the optimum load is plotted in Fig. 21. In the same figure the rectifier input power is shown, which is lower than the received one due to the loaded-filter insertion loss, that is 11 dB in the presence of the ethanol solution and higher when the channel is filled with other fluids. From these figures the rectifier sensitivity can be derived: while a dc output is observed with a minimum rectifier input power of -26 dBm (at -15 dBm of received power in Fig. 21), the rectifier capability of acting also as an ethanol-solution detector, showing an evident separation between the curves, occurs for a minimum rectifier input power of -20 dBm (at -10 dBm of received power in Fig. 21). In fact, in such conditions the dc output voltage in the absence of the ethanol solution is up to one half the value obtained when the channel is filled with it (at -10 dBm of received power in Fig. 20).

The final geometrical parameters are compared to the ones of the reference unloaded filter in Table II.
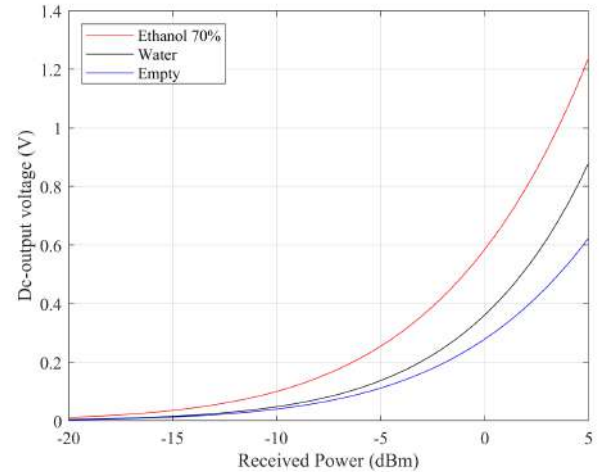

Fig. 20. Dc-output voltage for different fluids filling the channel.

In the first section, the upper line width is maintained at its original to match the one of the antenna feeding line. In the second section, the use of the modified open stub in place of an open end resulted in a different coupled lines length, to keep the same filter behavior at 2.45 GHz, while the width has been significantly reduced, which in certain cases becomes one third of the original ones. These geometrical parameters variation is also justified by the integrated filter design to act also as a matching network between the antenna and the nonlinear rectifier. Furthermore, the coupled line gap is increased from 0.1 mm to 0.4 mm for the first section and from 0.1 mm 0.25 mm for the second section: this parameter resulted to play an important role in enhancing the discrimination of the three fluids in terms of dc-output voltage curves.
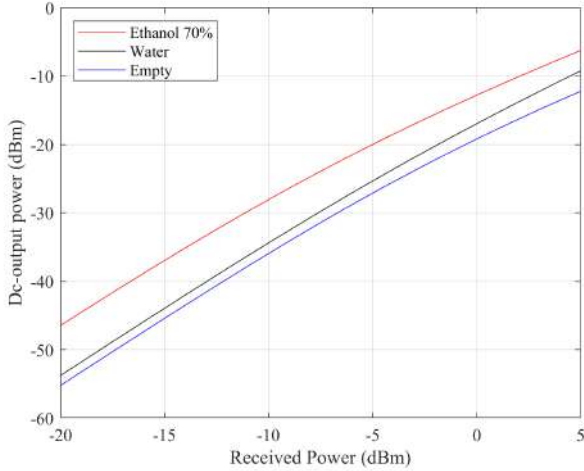
Fig. 21. Rectifier RF-input and dc-output power versus impinging power for different fluids filling the channel.

Fig. 22. PI and VI rectenna characteristics in stationary conditions, for a received power of 0 dBm.

TABLE II
FILTENNA OPTIMIZED VALUES

Component	Filter	Loaded filter
$W1_{sup}$	1.5 mm	1.5 mm
$W1_{inf}$	1.5 mm	0.47 mm
$W2_{sup}$	1.5 mm	0.5 mm
$W2_{inf}$	1.5 mm	0.7 mm
$W3$	1.5 mm	0.85 mm
$s1$	0.1 mm	0.4 mm
$s2$	0.1 mm	0.25 mm
$L1$	22.3 mm	28.9 mm
$L2$	22.3 mm	21.7 mm
$L3$	10 mm	17 mm

To evaluate the overall performance of the sensor, the behavior at the system dc output, in terms of power and voltage in variable loading conditions [30], has been derived and a representative plot, for a received power of 0 dBm, is reported in Fig. 22. In this case the channel is filled with the ethanol solution. By Fig. 22 inspection it is clear that the load optimized value used (dashed line in the figure) does not correspond to the one for the maximum dc output power. This is due to the fact that the optimization focus has been given to a trade-off between the RF-to-dc power transfer efficiency of the overall system and the capability to have different appreciable dc-output voltages related to the tested fluids.

These two goals are strictly dependent on the filter geometrical parameters and in particular to the separation factor "s": a value of 0.1 mm would have brought the system to show higher performance in terms of dc-output voltage, but with less distinguishable values for the three filling fluids.

When the filter is optimized within a nonlinear simulation, the matching between the antenna and the rectifier is correctly performed by the filter itself. In order to have a rough representation of the filter behavior after the optimization, the S-parameters are computed using Z_A and the rectifier input impedance at -10 dBm (see Fig. 15), respectively, as
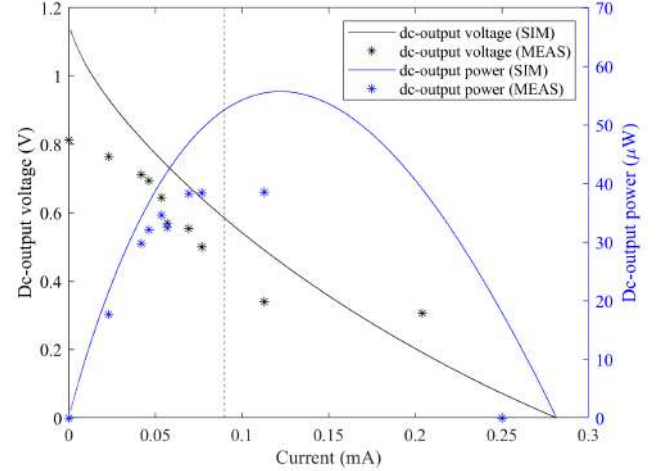
the ports terminations. This computation is performed both for the loaded filter circuit model and for its EM simulation. The corresponding results are depicted in Fig. 23, Fig. 24 and Fig. 25.
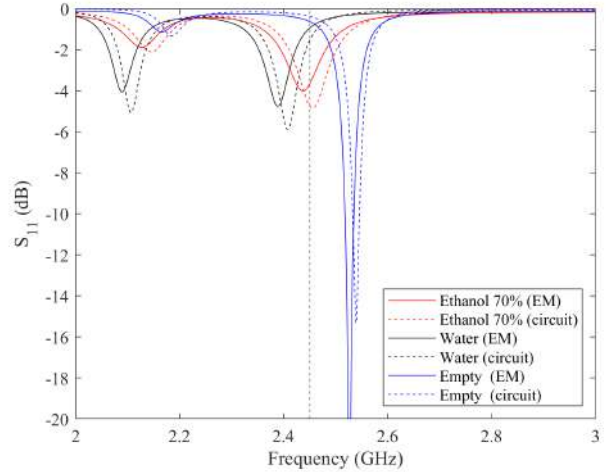

Fig. 23. Reflection coefficient of the filter input port for the different fluids filling the channel: comparison between full-wave and circuital simulations.

As the graphs display, in the presence of the ethanol solution the filter resonates around 2.45 GHz and the performance in terms of reflection and transmission coefficients are appreciably different for the other compared fluids. The substitution of one open end with the designed stub induces a degradation on the performance the filter would have in case of the stand-alone coupled-line one. However, a coherent selective behavior at the desired frequency is achieved, highlighting how the different impedances of the three resonant stubs at the operating frequency allow sub-optima results.

Finally the system output performance have been investigated with respect to different ethanol concentrations, whose permittivity and conductivity have been derived from [24]. The results are reported in Table III (for an impinging power
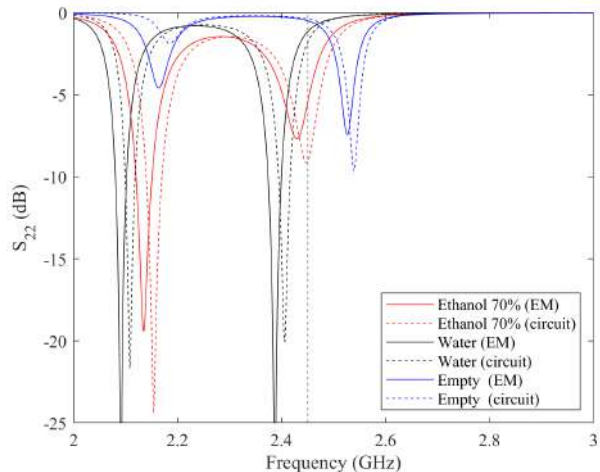
Fig. 24. Reflection coefficient of the filter output port for the different fluids filling the channel: comparison between full-wave and circuital simulations.
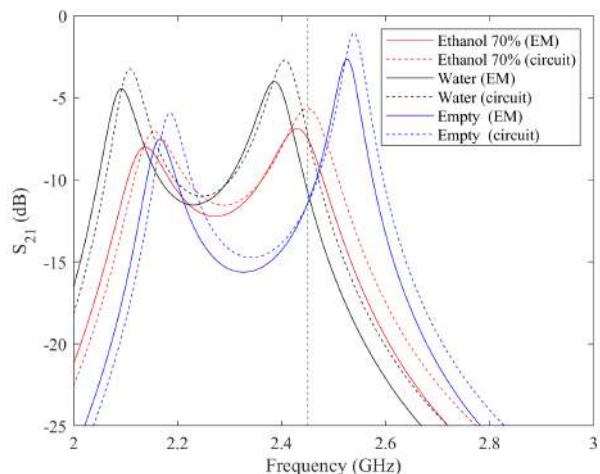

Fig. 25. Transmission coefficient of the filter for the different fluids filling the channel: comparison between full-wave and circuital simulations.

of 0 dBm) and show that the targeted 70% ethanol solution results in an output dc voltage fully distinguishable from lower concentrations.

TABLE III
DC-OUTPUT VOLTAGES FOR DIFFERENT WATER-ETHANOL SOLUTIONS

Ethanol concentration (%)	ε_r	σ	dc-output voltage
30%	60	2.45	0.420 V
40%	52	2.45	0.463 V
50%	44	2.45	0.508 V
60%	33.5	2.18	0.585 V
70%	30	2.18	0.586 V
80%	22.8	1.91	0.608 V
90%	16	1.63	0.571 V

Furthermore, as anticipated in Section II, the dc-output voltages are computed for the condition of having a half-filled channel and different ethanol concentrations. Fig. 26 shows

how these cases allow to safely detect the presence of ethanol despite of the half-filled channel. The simulated values are compared to the reference one, represented by the channel completely filled with the ethanol solution 70% concentration.
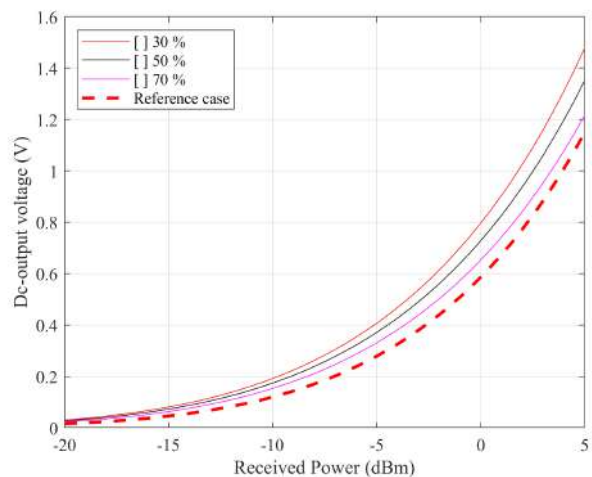

Fig. 26. Dc-output voltage levels for a half-filled channel with different ethanol concentration, compared to the reference case.

V. RESULTS AND MEASUREMENTS

The photo of the front view of the realized prototype is shown in Fig. 27(a), whereas Fig. 27(b) displays the microfluidic channel derived in the system ground plane. The chosen technology with the ground plane allows to keep the designed wearable system, except from the microfluidic channel, completely decoupled from the human body.

Before measuring the system performance in terms of sensing, every single subcomponent has been characterized. At first, the patch antenna is characterized by using a VNA (Vector Network Analyzer) to verify the correct tuning after the prototyping procedures; the results are shown in Fig. 28. The corresponding radiation diagrams are then measured, first in air and then as it was placed on a human arm. The measured radiations diagrams are displayed in Fig. 29. As shown, the presence of the skin behind the antenna has influenced the front-to-back ratio, but does not affect its broadside behavior.

Subsequently, the filter is characterized using the VNA to measure the related scattering parameters in the presence of the tested fluids. Since the filter is connected to the VNA through two 50- Ω connectors, the simulated full-wave filter scattering parameters are re-normalized with respect to 50- Ω terminations, for comparison purposes and the results are shown in Fig. 30- Fig. 32. As it can be noticed, the realized filter, measured for various fillings of the channel, shows a slight detuning with respect to the simulated one: thus the center frequencies of the prototype are 2.31 GHz for ethanol, 2.22 GHz for water and 2.46 GHz when the channel is empty. This discrepancy, with respect to the simulations, is a consequence of a nonlinear/EM co-simulations that takes into account a diode model with parasitic elements related to the diode package that could be not accurately estimated.
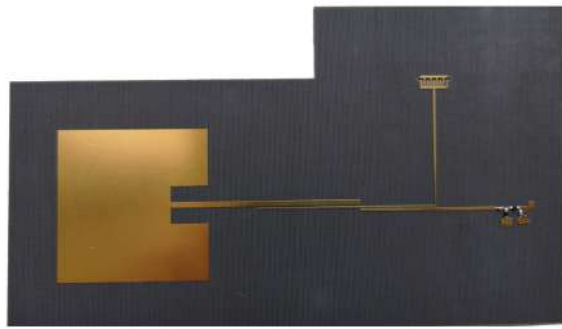
(a)
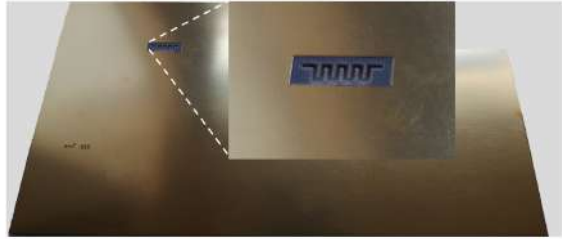
(b)

Fig. 27. Realized prototype of the proposed filtenna: (a) front view hosting the filtenna and rectifier, and (b) back view with a close-up on the microfluidic channel.
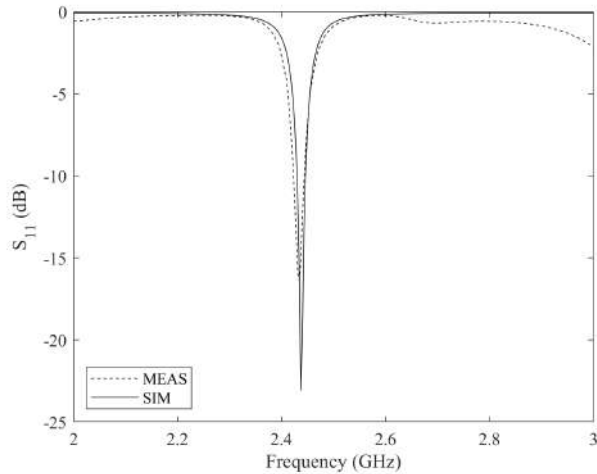

Fig. 28. Antenna input reflection coefficient: simulations and measurements comparison.

In fact, during the measurements the operating frequency of the filter is confirmed to be 2.3 GHz, with high repeatability. This is confirmed by the simulations carried out at 2.3 GHz that are in agreement with the measurements. To correctly quantify the received power, the filter loaded by the rectifier has been connected to the RF-generator, and the dc-output voltage is measured for increasing RF-power, first in open-circuit loading conditions and then with the optimum load of 6500 Ω. These values are compared with the simulated ones, without considering the parasitic elements inside the diode model, and are reported in Fig. 33 and Fig. 34. The results are in very good agreement all over the entire power range and the different fluids fillings are clearly detectable. To ensure
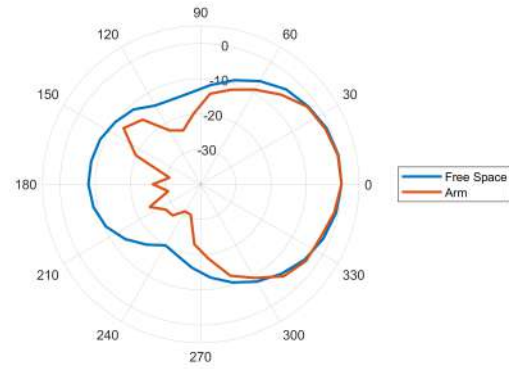

Fig. 29. Radiation diagram for the designed patch antenna: the blue curve represents a measurement in air and the red one when the antenna is placed on an arm.

Fig. 30. Reflection coefficient at the filter input port: full-wave simulated and measurement results for the different fluid filling the channel.

Fig. 31. Transmission coefficient of the filter: full-wave simulated and measurement results for the different fluid filling the channel.
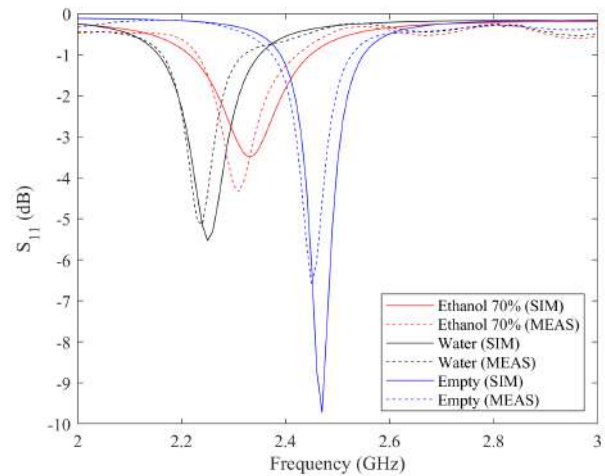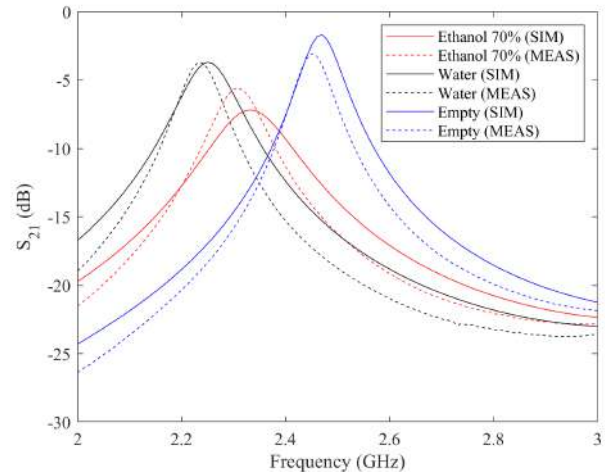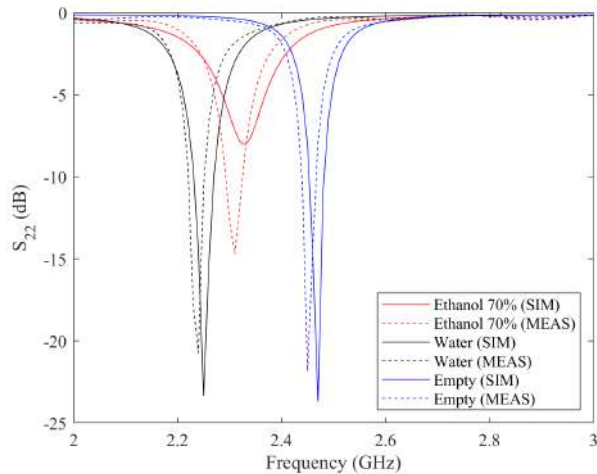
Fig. 32. Reflection coefficient at the filter output port: full-wave simulated and measurement results for the different fluid filling the channel.
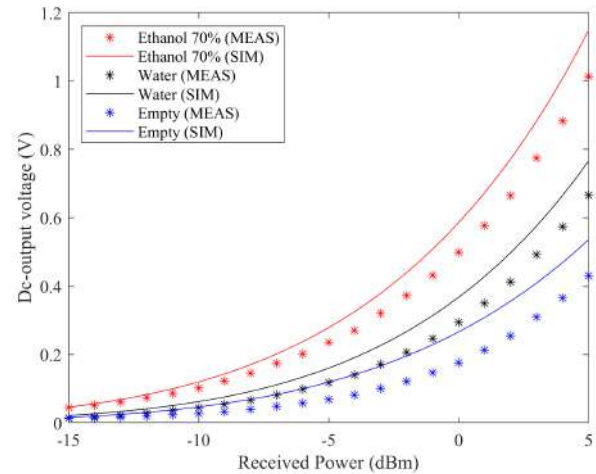

Fig. 34. Measured dc-output voltage on the optimum load for the different fluids filling the channel.

absence of ambiguity, the power source and the system should be in a line-of-sight condition at a fixed distance, in this way the received power is well determined. A controlled gate is foreseen, in which a person wearing the bracelet is asked to place the hand to perform the reading, after the use of an alcohol-based hand sanitizer.

Fig. 35. Photo of the laboratory setup used to mimic a controlled gate for ethanol detection: the distance between the RF-power source and the detector is fixed (the hand positioning on the x-y plane can vary)
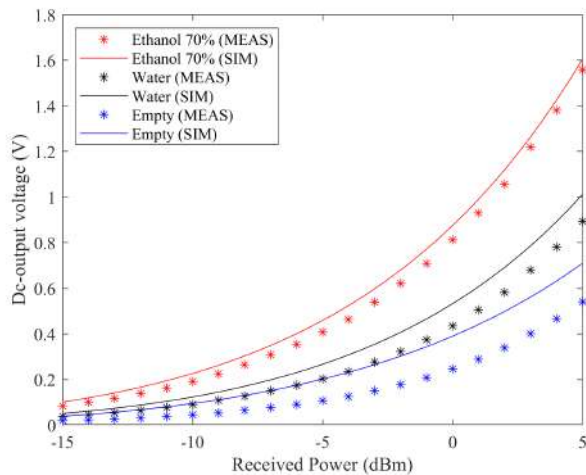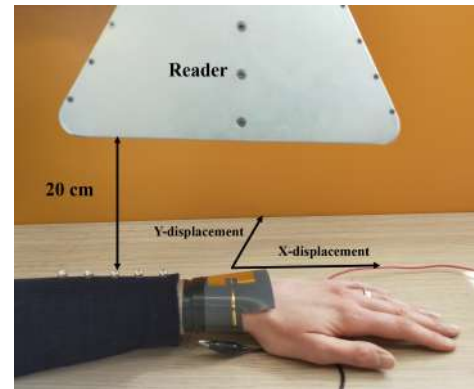

Fig. 33. Measured dc-output voltage, on an open circuit load, for different fluids filling the channel.

This is depicted in Fig. 35 where a horn antenna, for RF-power transmission is located at 20 cm from the bracelet; for the following measurements a received power of -10 dBm is considered.

Using this set-up, the system robustness to possible displacements with respect to the Tx antenna has been checked: starting from the Tx and Rx antennas geometrical centers perfectly aligned, the bracelet has been moved with top-bottom and left-right displacements of up to 4 cm. The measured dc-output voltages for x- and y- displacements (see Fig. 35) are reported in Figs. 36(a) and (b), respectively: in both cases it can be concluded that the detection of ethanol solution is

preserved regardless of such large positioning uncertainties, thus demonstrating the feasibility of the proposed wearable system.

VI. CONCLUSION

In this work, we have presented the design and the experimental validation of a wearable, wirelessly activated system for the detection of ethanol solutions. The system is realized on a flexible substrate and makes use of a 2.45 GHz patch antenna connected to a coupled-line loaded filter. One of the filter open ends is substituted with a stub embedding a microfluidic channel. The stub resonates as an open circuit at 2.45 GHz only in the presence of a water-ethanol solution. In this way, it is demonstrated that the system selectively differentiates an ethanol solution, of 70% concentration, from water or air. The filter output is connected to a rectifier and the ethanol solution is discriminated in terms of dc-output voltages on the rectifier optimum load. The whole system is optimized by coupling full-wave analysis, of both the antenna and the loaded, with nonlinear circuit optimization. Its ability to detect the solution is predicted in real conditions, demonstrating its robustness
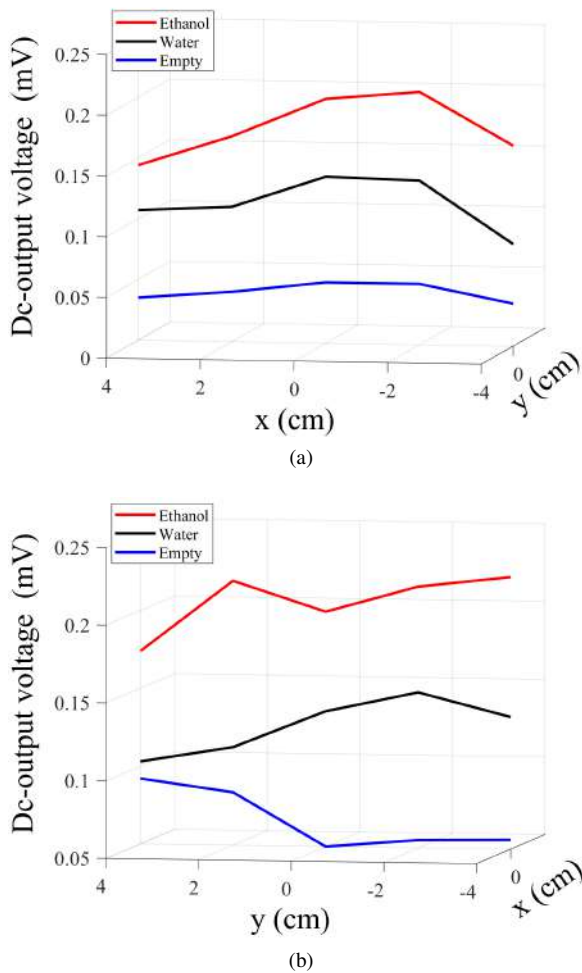
Fig. 36. Measured dc-output voltage, on an open circuit load, for different fluids filling the channel, in case of misalignements between the RF source and the bracelet: (a) x-misalignment, (b) y-misalignment.

with respect to partial fillings of the microfluidic channel, that cannot be avoided as in controlled laboratory experiments. The operations of the ethanol detector have been confirmed by the experimental results, although a slight shift of the nominal operating frequency has been observed.

REFERENCES

[1] J. Leroy ,C. Dalmay, A. Landoulsi, F. Hjeij, C. Mlin, B. Bessette, C. Bounaix Morand du Puch, S. Giraud, C. Lautrette, S. Battu, F. Lallou, M.O. Jauberteau, A. Bessaudou, P. Blondy, A. Pothier, "Microfluidic biosensors for microwave dielectric spectroscopy," *Sens. Actuators A, Phys.*, vol. 229, pp. 172-181, Jun. 2015.

[2] K. Grenier, D. Dubuc, T. Chen, F. Artis, T. Chretiennot, M. Poupot, J.-J. Fourni, "Recent Advances in Microwave-Based Dielectric Spectroscopy at the Cellular Level for Cancer Investigations," *IEEE Trans. Microw. Theory Techn.*, vol. 61, no. 5, pp. 2023-2030, May 2013.

[3] L. Corchia, G. Monti, E. D. Benedetto and L. Tarricone, "A Chipless Humidity Sensor for Wearable Applications," in *Proc. RFID-TA*, Pisa, Italy, 2019, pp. 174-177.

[4] A. A. Helmy, S. Kabiri, M. M. Bajestan and K. Entesari, "Complex Permittivity Detection of Organic Chemicals and Mixtures Using a 0.53-GHz Miniaturized Spectroscopy System," *IEEE Trans. Microw. Theory Techn.*, vol. 61, no. 12, pp. 4646-4659, Dec. 2013.

[5] N. Wiwatcharagoses, K. Y. Park, J. A. Hejase, L. Williamson and P. Chahal, "Microwave artificially structured periodic media microfluidic sensor," in *Proc. ECTC*, Lake Buena Vista, FL, USA, 2011, pp. 1889-1893.

[6] L.Dai *et al.*, "Microfluidics-based microwave sensor," *Sens. Actuators A, Phys.*, vol. 309, 2020.

[7] H. Hamzah, J.Lees, A.Porch, "Split ring resonator with optimised sensitivity for microfluidic sensing," *Sens. Actuators A, Phys.*, vol. 276, pp. 1-10, Jun. 2018.

[8] A. Cataldo, L. Catarinucci, L. Tarricone, F. Attivissimo and E. Piuzzi, "A Combined TDFD Method for Enhanced Reflectometry Measurements in Liquid Quality Monitoring," *IEEE Trans. Instrum. Meas.*, vol. 58, no. 10, pp. 3534-3543, Oct. 2009.

[9] C. Dalmay, M. Cheray, A. Pothier, F. Lallou, M.O. Jauberteau, P. Blondy, "Ultra sensitive biosensor based on impedance spectroscopy at microwave frequencies for cell scale analysis," *Sens. Actuators A, Phys.*, vol. 162, no. 2, pp.189-197, Aug. 2010.

[10] K. Grenier, D. Dubuc, P. Poleni, M. Kumemura, H. Toshiyoshi, T. Fujii and H. Fujita, "Integrated Broadband Microwave and Microfluidic Sensor Dedicated to Bioengineering," *IEEE Trans. Microw. Theory Techn.*, vol. 57, no. 12, pp. 3246-3253, Dec. 2009.

[11] T. Chen, D. Dubuc, M. Poupot, J. Fournie and K. Grenier, "Accurate Nanoliter Liquid Characterization Up to 40 GHz for Biomedical Applications: Toward Noninvasive Living Cells Monitoring," *IEEE Trans. Microw. Theory Techn*, vol. 60, no. 12, pp. 4171-4177, Dec. 2012.

[12] T. Chretiennot, D. Dubuc and K. Grenier, "A Microwave and Microfluidic Planar Resonator for Efficient and Accurate Complex Permittivity Characterization of Aqueous Solutions," *IEEE Trans. Microw. Theory Techn.*, vol. 61, no. 2, pp. 972-978, Feb. 2013.

[13] T. Chretiennot, D. Dubuc and K. Grenier, "Double stub resonant biosensor for glucose concentrations quantification of multiple aqueous solutions," in *IEEE MTT-S Int. Microw. Symp.*, Tampa, FL, USA, 2014, pp. 1-4.

[14] T. Chretiennot, D. Dubuc and K. Grenier, "Optimized electromagnetic interaction microwave resonator/microfluidic channel for enhanced liquid bio-sensor," in *Proc. EuMC*, Nuremberg, 2013, pp. 464-467.

[15] T. Chen, D. Dubuc, M. Poupot, J. Fourni and K. Grenier, "Broadband discrimination of living and dead lymphoma cells with a microwave interdigitated capacitor," in *Proc. BioWireleSS* , Austin, TX, USA, 2013, pp. 64-66.

[16] B. S. Cook, J. R. Cooper and M. M. Tentzeris, "An Inkjet-Printed Microfluidic RFID-Enabled Platform for Wireless Lab-on-Chip Applications," *IEEE Trans. Microw. Theory Techn.*, vol. 61, no. 12, pp. 4714-4723, Dec. 2013.

[17] G. M. Rocco, M. Bozzi, S. Marconi, G. Alaimo, F. Auricchio and D. Schreurs, "3D-Printed Microfluidic Sensor in Substrate Integrated Waveguide Technology," in *Proc. IMWS-AMP*, Ann Arbor, MI, USA, 2018, pp. 1-3.

[18] B. D. Wiltshire and M. H. Zarifi, "3-D Printing Microfluidic Channels With Embedded Planar Microwave Resonators for RFID and Liquid Detection," in *IEEE Microw. Wireless Compon. Lett.*, vol. 29, no. 1, pp. 65-67, Jan. 2019.

[19] I. Piekarz, J. Sorocki, K. Wincza and S. Gruszczynski, "Effective permittivity measurement with the use of coupled-line section sensor," in *Proc. RWS*, Austin, TX, USA, 2016, pp. 165-168.

[20] C. Lee, B. Bai, Q. Song, Z. Wang and G. Li, "Open Complementary Split-Ring Resonator Sensor for Dropping-Based Liquid Dielectric Characterization," *IEEE Sensors J.*, vol. 19, no. 24, pp. 11880-11890, Dec.15, 2019.

[21] A. Ebrahimi, J. Scott and K. Ghorbani, "Ultrahigh-Sensitivity Microwave Sensor for Microfluidic Complex Permittivity Measurement," *IEEE Trans. Microw. Theory Techn.*, vol. 67, no. 10, pp. 4269-4277, Oct. 2019.

[22] F. Benassi, N. Zincarelli, D. Masotti and A. Costanzo, "A wearable passive microwave fluid sensor wirelessly activated," in *Proc. WPTC 2019*, London, UK, 2019.

[23] A. Costanzo and D. Masotti, "Energizing 5G: Near- and Far-Field Wireless Energy and Data Trantransfer as an Enabling Technology for the 5G IoT," *IEEE Microw. Mag*, vol. 18, no. 3, pp. 125-136, May 2017.

[24] Bao, JianZhong, Mays L. Swicord, and Christopher C. Davis. "Microwave dielectric characterization of binary mixtures of water, methanol, and ethanol," *J. Chem. Phys.*, vol. 104 (12), 1996, pp. 4441-4450.

[25] D. M. Pozar, "Microwave Engineering," 4th ed., Wiley, 2011, New York, New York.

[26] V. Rizzoli, A. Costanzo and G. Monti, "General electromagnetic compatibility analysis for nonlinear microwave integrated circuits," in *IEEE MTT-S Int. Microw. Symp. Dig.*, Fort Worth, TX, USA, Jun. 2004, pp. 953-956 Vol.2.

[27] V. Rizzoli, A. Costanzo, D. Masotti, P. Spadoni and A. Neri, "Prediction of the End-to-End Performance of a Microwave/RF Link by Means

of Nonlinear/Electromagnetic Co-Simulation," *IEEE Trans. Microw. Theory Techn.*, vol. 54, no. 12, pp. 4149-4160, Dec. 2006.

[28] A. Costanzo, D. Masotti, M. Fantuzzi and M. Del Prete, "Co-Design Strategies for Energy-Efficient UWB and UHF Wireless Systems," *IEEE Trans. Microw. Theory Techn.*, vol. 65, no. 5, pp. 1852-1863, May 2017.

[29] T. Jensen, V. Zhurbenko, V. Krozer and P. Meincke, "Coupled Transmission Lines as Impedance Transformer," *IEEE Trans. Microw. Theory Techn.*, vol. 55, no. 12, pp. 2957-2965, Dec. 2007.

[30] D. Masotti, A. Costanzo, P. Francia, M. Filippi and A. Romani, "A Load-Modulated Rectifier for RF Micropower Harvesting With Start-Up Strategies," *IEEE Trans. Microw. Theory Techn.*, vol. 62, no. 4, pp. 994-1004, Apr. 2014.

Alessandra Costanzo is full Professor at Alma Mater Studiorum, Universit di Bologna, Italy, since 2018 where she leads the RF and wireless lab. She is currently involved in research activities dedicated to design entire wireless power transmission systems, based on the combination of EM and nonlinear numerical techniques, adopting both far-field and near-field solutions, for several power levels and operating frequencies. She has authored more than 260 scientific publications on peer reviewed international journals and conferences and several chapter books. She owns four international patents. She was co-founder of the EU COST action IC1301 WiPE Wireless power transfer for sustainable electronics. She is the past-chair (2016-2017) of the MTT-26 committee on wireless energy transfer and conversion and member of the MTT-24 committee on RFID. She is past Associate Editor of the IEEE Transaction on MTT, and Associate Editor of the Cambridge International Journal of Microwave and of Wireless Technologies. Since 2016 she has been Steering Committee Chair of the new IEEE Journal of RFID. She is MTT-S representative and Distinguished Lecturer of the CRFID, where she has been appointed Chair of EUMC2022

Francesca Benassi (GS'18) received a M.Sc. Degree in Biomedical Engineering from the University of Bologna, Italy, in 2017. She joined the Interdepartmental Center for Industrial ICT Research (CIRI ICT) of the University of Bologna in 2017 as a Research Fellow within the EU-supported HABITAT Project. Since 2018, she has been enrolled in the Electronics, Telecommunications, and Information Technologies Engineering Ph.D. programme, working within the framework of the PRIN WPT4WID ("Wireless Power Transfer for Wearable and Implantable Devices") project. Her research interests include the design of Wireless Power Transfer systems operating at microwaves and millimeter-waves for both wearable and implantable biomedical devices and microwave systems for fluid detection. In 2021, she received the MTT-S Graduate Fellowship Award.

Giacomo Paolini (GS'18) received the M.Sc. Degree in Biomedical Engineering and the Ph.D. Degree in Electronics, Telecommunications, and Information Technologies Engineering from the University of Bologna, Italy, in 2016 and 2021, respectively. He joined the Interdepartmental Center for Industrial ICT Research (CIRI ICT) of the University of Bologna as a research fellow within the EU-supported HABITAT project in 2016. He is currently working as a postdoctoral researcher at the Department of Electrical, Electronic and Information Engineering G. Marconi (DEI) of the University of Bologna, working within the framework of the PRIN WPT4WID ("Wireless Power Transfer for Wearable and Implantable Devices") project. His research interests include microwave radar systems for biomedical applications, indoor positioning exploiting RFID technologies and far-field wireless power transfer systems.

Diego Masotti (M'00, SM'16) received the Ph.D. degree in electric engineering from the University of Bologna, Italy, in 1997. In 1998 he joined the University of Bologna and is now Associate Professor of electromagnetic fields. His research interests are in the areas of nonlinear microwave circuit simulation and design, with emphasis on nonlinear/electromagnetic co-design of integrated radiating subsystems/systems for wireless power transfer and energy harvesting applications. He authored more than 70 scientific publications on peer reviewed international journals and more than 130 scientific publications on proceedings of international conferences. Dr. Masotti serves in the Editorial Board of the International Journal of Antennas and Propagation, the Journal of Wireless Power Transfer, IEEE Access, and Electronics Letters and is a member of the Paper Review Board of the main Journals of the microwave sector.